Kebaïli and Dammak *Journal of Theoretical and Applied Physics* 2012, **6**:21
http://www.jtaphys.com/content/6/1/21

Journal of Theoretical and Applied Physics
a SpringerOpen Journal

RESEARCH Open Access

Theoretical analysis and intensity calculation for the $f \rightarrow d$ absorption spectrum of Ce^{3+} in $YAl_3(BO_3)_4$ crystal

Imen Kebaïli and Mohamed Dammak*

Abstract

Emission, absorption, and excitation spectra of $4f \rightarrow 5d$ transitions of Ce^{3+} ions in yttrium aluminum borate (YAB) crystal are reviewed and successfully reproduced by theoretical investigations. The Ce^{3+} energy level diagram has been compiled after a careful analysis of the optical spectra. Theoretical calculations based on free ion and crystal field Hamiltonians are used to interpret the observed transitions. The $4f$ and $5d$ crystal field parameter permits determination of the engine states of Ce^{3+} ion in YAB and then calculating the absorption line intensities as well as the effective section and the decay times.

Keywords: Crystal-field, Intensity calculation, Decay time, YAB: Ce^{3+}

Background

The $4f^N \rightarrow 4f^{N-1}5d$ transitions of lanthanide ions have been extensively studied due to their important role in many luminescent devices [1,2]. Dorenbos et al. have made an extensive compilation of the experimental data for these transitions, from which a semi-empirical model has been proposed [3,4]. It was demonstrated that once the energy difference between the lowest $5d$ and $4f$ levels of a Ln^{3+} ion is known for a given crystal, then such energy difference for all other Ln^{3+} ions in the same crystal can be predicted by the model quite accurately. The $Ce^{3+}5d \rightarrow 4f$ transitions are allowed by both spin and parity selection rules with a short radiative lifetime of about 10 to 50 ns, which is desirable for applications in scintillations, light-emitting diodes, and field emission displays [5-7].

In this article, optical properties of yttrium aluminum borate (YAB): Ce^{3+} is going to be further highlighted by a detailed theoretical study. The emission, absorption, and excitation spectra of Ce^{3+} doped in yttrium aluminum borate ($YAl_3(BO_3)_4$) single crystals are recently reported [8]. The polarized emission spectrum permits determination of the $^2F_{5/2}$ Stark splitting in agreement with EPR results [8]. However, these levels were not characterized with respect to symmetry type, and no attempt was made to analyze the observed energy level structure in terms of model crystal field Hamiltonian. Based on our recent works on rare earth ions in YAB, Er^{3+} [9], Yb^{3+} [10], and Tm^{3+} [11], we present a detailed crystal field investigation for Ce^{3+} ion in YAB in order to interpret the different spectra. Using the eigenvectors of the crystal field levels originating from $4f$ and $5d$ configurations, the absorption intensity peaks are reasonably well simulated, and the calculated decay time of the $5d \rightarrow {}^2F_{5/2}$ emissions will be compared with experimental value.

Crystal structure

YAB belongs to the double borate family which crystallizes in the trigonal structure of the mineral $CaMg_3(CO_3)_4$ and belongs to the R_{32} space group. The yttrium occupies sites in trigonal prisms, whereas the aluminum and boron atoms are situated, respectively, in the octahedrons and triangles of oxygen with cell parameters $a = b = 9.295$ Å and $c = 7.243$ Å, $Z = 3$ [12]. Indeed, the Y^{3+} ions can be replaced by other trivalent RE ions to give optically active materials [13]. Ce^{3+} replaces Y^{3+} in sites through sixfold oxygen coordination and trigonal geometry with D_3 point symmetry. The Al^{3+} ions are in octahedral sites, whereas the B^{3+}

* Correspondence: madidammak@yahoo.fr
Université de Sfax, Faculté des Sciences de Sfax, Département de Physique, Laboratoire de Physique Appliquée, Groupe de Physique Théorique, Sfax 3018, Tunisia

ones are surrounded by three oxygen atoms with triangular geometry.

Theory

Matrix elements of Hamiltonians

The single electron Hamiltonian is given by:

$$H = H_0 + H_{\mathrm{SO}} \tag{1}$$

where H_0 is the electrostatic Hamiltonian translating the Coulomb interactions with the nucleus, and H_{SO} is the traditional spin-orbit coupling Hamiltonian.

$$H_{\mathrm{so}} = \xi_f \overrightarrow{1.S} \tag{2}$$

In the absence of H_{SO}, the Ce^{3+} ion possesses [s.c.c] 4*f* configuration as fundamental state and [s.c.c] 5*d* configuration as first excited state. The 4*f* fundamental level with ^2F spectral term is separated into two multiplets: $^2F_{5/2}$ and $^2F_{7/2}$ under the influence of the spin-orbit coupling with an energy difference of about 2,500 cm^{-1}. According to Hund's rules, the fundamental state is $^2F_{5/2}$. The ^2D first excited term splits into two multiplets: $^2D_{3/2}$ and $^2D_{5/2}$.

Due to the action of the crystal field Hamiltonian with D_3 symmetry, the $(2J + 1)$ fold degeneracy of the free ion states is lifted in a way that is predictable by group theory. The number of the Stark components of a $^{2S+1}L_J$ state of Ce^{3+} is $(2J + 1)$, and each sublevel may be classified as having either $E_{1/2}$ or $E_{3/2}$ symmetry in D_3 rotation group.

The number and symmetry of the resulting states are expressed by the full rotation compatibility table (Table 1). Selection rules for electric dipole transitions can then be deduced by group theory considerations (Table 2).

The crystal field Hamiltonian describing 4*f* and 5*d* configuration states is given by:

$$H_{\mathrm{CF}} = \sum_{\mathrm{k,q}} B_{\mathrm{kq}} C_{\mathrm{kq}} \tag{3}$$

In the case of a crystal field with D_3 symmetry, only six real crystal field parameters (CFPs) are nonzero for the 4*f* configuration:

Table 1 Rotation compatibility table of the D_3' double group

J	E^a
3/2	$E_{1/2} + E_{3/2}$
5/2	$2E_{1/2} + E_{3/2}$
7/2	$3E_{1/2} + E_{3/2}$

Table 2 Polarized electric dipole transition selection rules for the D_3' double group

	$E_{1/2}$	$E_{3/2}$
$E_{1/2}$	π, б	б
$E_{3/2}$	б	π

$$\hat{H}_{CF} = B_2^0\hat{C}_2^0 + B_4^0\hat{C}_4^0 + B_4^3\left(\hat{C}_4^{-3} - \hat{C}_4^3\right) + B_6^0\hat{C}_6^0 + B_6^3\left(\hat{C}_6^{-3} - \hat{C}_6^3\right) + B_6^6\left(\hat{C}_6^6 + \hat{C}_6^{-6}\right) \tag{4}$$

The energy level simulation is usually carried out considering simultaneously both free ion and crystal field effects. The details of the fitting procedure are reported in reference [9]. The starting values of the 4*f* CFPs have been calculated by averaging over the values reported for the Er^{3+}, Yb^{3+}, and Dy^{3+} in YAB [9,10,14]. All parameters have then been allowed to vary freely in order to minimize the difference between experimental and theoretical Stark energy levels.

The above Hamiltonian can also be utilized for the 5*d* configuration. In this case, the sixth-order crystal field terms B_6^0, B_6^3, and B_6^6 are equal to 0, and the spin-orbit coupling constant is $\xi_d(r)$.

However, unlike the 4*f* configuration, the 5*d* configuration experiences a crystal field interaction that is considerably larger because 5*d* electrons are directly exposed to the host crystal field. In our case, we have considered the entire Hamiltonian with no approximation in order to calculate the 4*f* and 5*d* energy levels.

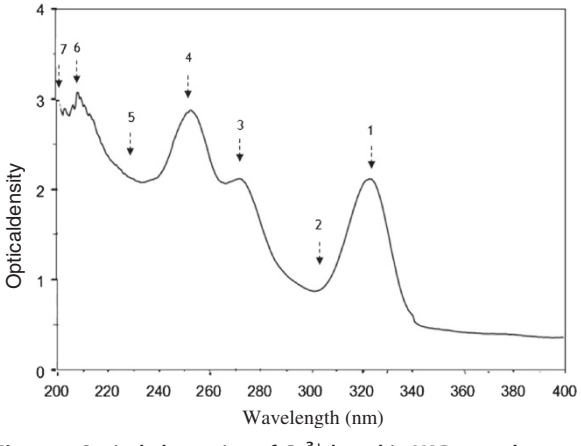

Figure 1 Optical absorption of Ce^{3+}doped in YAB crystal measured at 300 K [8].

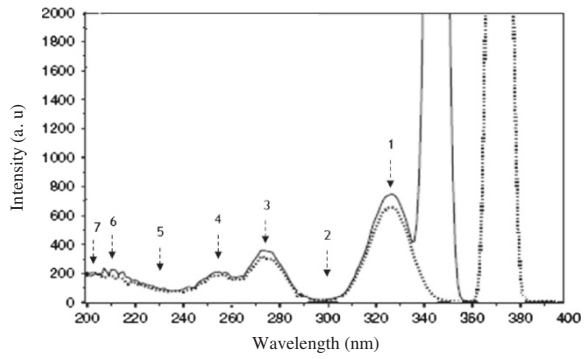

Figure 2 Excitation spectra of YAB-doped Ce^{3+}measured at 300 K. Emission is measured at 345 nm (continuous curve) and at 371 nm (dashed curve) [8].

Matrix elements of $f^N \rightarrow f^{N-1}d$transitions

The interconfiguration transitions are allowed in the order of electric dipole transitions. They can be correctly described by considering that their intensities are proportional to the square of the constituents of electric dipole estimated between the final and the initial states. The electric dipole is given by:

$$\overrightarrow{D} = \sum_{i=1}^{n} -e\overrightarrow{r_i} \tag{5}$$

where $\rightarrow r_i$ is the position of the ith electron.

The I_{if} unpolarized transition intensities of zero-phonon lines between the 4*f* and 5*d* levels is expressed as:

$$I_{if} \propto v_{if} \left\langle \psi_{4f^{N-1}5d} \middle| D_q^1 \middle| \psi_{4f^1} \right\rangle^2 \tag{6}$$

where ϑ_{if} is the zero-phonon line transition wave number, Dq is the electric dipole operator, and the summation is over the polarization q ($q = 0, \pm 1$).

These matrix elements were calculated using the pure electronic wave functions obtained by the energy level calculations for 4*f* and 5*d* configurations. In the calculation, we made the approximation that the $f \rightarrow d$ transition intensity is proportional to the zero-phonon line energy. The matrix elements are calculated between starting level states [15]:

$$\left\langle 4f^{N-1}5d, \alpha, L, S, J, M_J \middle| D_q^1 \middle| 4f^1, \alpha', L', S', J', M_J' \right\rangle \tag{7}$$

Radiatif lifetime and oscillator strength

The decay time is a significant parameter to estimate the efficiency of a laser system. This decay time τ between i and i' states is given by:

$$\tau = \frac{1}{A_{ii'}} \tag{8}$$

where $A_{ii'} = \frac{64\pi^2 e^2 k_{ii'}^3 n(k_{ii'})}{3hg_i} S_{ii'} = 7.235610^{10} \frac{k_{ii'}^3 n(k_{ii'})}{g_{i'}} S_{ii'}$ (9)

$A_{ii'}$ is the probability of spontaneous transition between the degenerated levels in the condensed materials [16,17], $n(k_{ii'})$ is the refractive index, $k_{ii'}$ is the wave number, $g_{i'}$ is the degeneration degree of the first excited state, and $S_{ii'}$ is the electric dipole transition line strength. The refractive index n is supposed to be equal to 1.72 because it's change is small in the $YAl_3(BO_3)_4$ crystals in the studied spectral range [10].

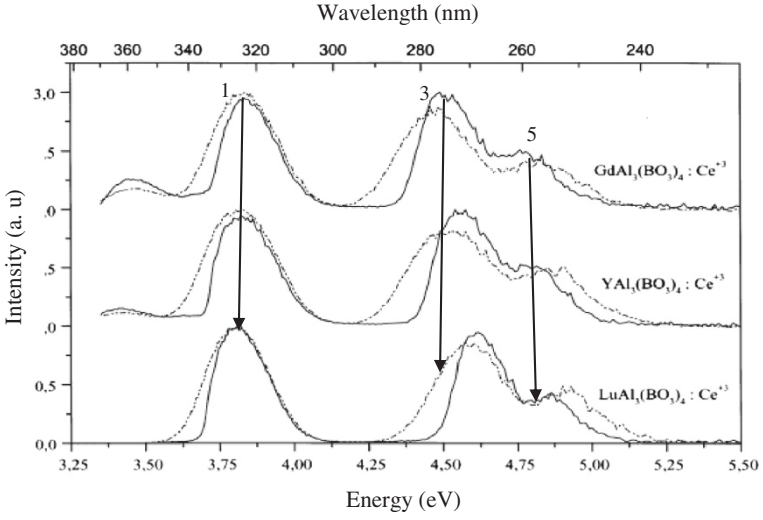

Figure 3 Excitation spectra of Ce^{3+}-doped $XAl_3(BO_3)_4$ crystals as function of temperature. Solid line, 30 K; dashed line, 300 K (*X* = Gd, Y, Lu) [20].

The electric dipole transition line strength between the i and $i\prime$ states is connected to the oscillator strength $f_{i\prime i}$ by the following quotient [18]:

$$S_{i'i} = \frac{3hg_i}{8\pi^2 mck_{i'i}} f_{i'i} = 0.92189410^{-11} \frac{g_i}{k_{i'i}} f_{i'i} \qquad (10)$$

where g_i is the degeneration degree of the first fundamental state.

Finally, the oscillator strength parameter is given by [19]:

$$f_{ii'} = 10^3 ln10 \frac{mc^2}{2e^2 N_A} \frac{3n}{n^2+2} I_{ii'} = 6.7810^{-9} \frac{3n}{n^2+2} I_{ii'} \qquad (11)$$

where $I_{ii'}$ is the intensity transition and N_A is the Avogadro number.

Results and discussion

Absorption and excitation spectra

The basis of our theoretical analysis will be the optical spectra of Ce^{3+} doped in YAB crystals [8,20]. The most careful study reported in the bibliography about this subject is that of Watterich et al. [8].

Figure 1 presents the absorption spectrum of cerium-doped YAB crystal realized at room temperature [8]. This spectrum extends over a spectral domain varying from 200 to 400 nm and can be decomposed to seven bands, labeled from 1 to 7. Five bands among them should be attributed to the electric dipole transitions from $^2F_{5/2}$ ground state to 5*d* levels.

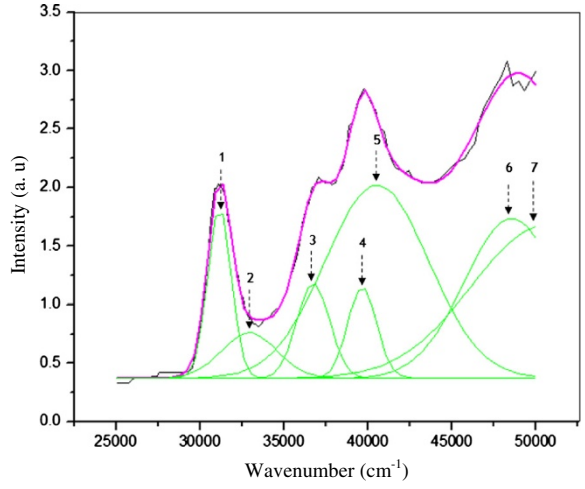

Figure 4 Deconvolution of the absorption spectrum of YAB-doped Ce^{3+}measured at 300 K. The green curves correspond to the deconvoluted absorption bands. The pink curve represents the absorption spectrum obtained by the deconvolution.

Table 3 Experimental energy levels and their corresponding intensities calculated from the absorption spectrum of YAB:Ce

Peak	Energy (cm^{-1})	Intensity (a. u)
1	31,152	1.4
2	32,934	0.38
3	36,741	0.81
4	39,657	0.78
5	40,533	1.64
6	48,561	1.36
7	50,535	1.3

(Figure 4, after deconvolution).

The excitation spectrum of YAB:Ce measured in the 200- to 400-nm range is presented in Figure 2. The seven detected bands correspond well with those detected in the absorption spectrum (Figure 1).

By considering the decomposition of 4*f* and 5*d* configurations under the influence of spin-orbit coupling and crystal field effect, we expected only five lines corresponding to transitions from the $^2F_{5/2}$ (F_1) fundamental state and the five Stark levels stemming from $^2D_{3/2}$ and $^2D_{5/2}$ multiplets. Indeed, the evolution of these peaks with temperature presents different behaviors. The peaks 1, 2, 4, 6, and 7 are not affected by the temperature variation; however, the peaks 3 and 5 are shifted to lower energies when increasing the temperature (Figure 3). These two emissions are then related to the YAB host, whereas 1, 2, 4, 6, and 7 peaks are related to the Ce^{3+} internal transitions, which are due to the electric dipole transitions from $^2F_{5/2}$ ground state to 5*d* levels.

The best deconvolution of the absorption spectrum is obtained for seven Gaussian bands (Figure 4). The experimental energy levels and intensities of each band are reported in Table 3.

It is worth noticing that the deconvolution of the absorption spectrum was realized by considering, in the first step, five bands and six bands; however, the energetic position and the intensity of each band obtained in these cases were not in agreement with theoretical calculations. For these reasons, we have considered seven

Table 4 Theoretical and experimental intensities of the lines of YAB:Ce^{3+} corresponding to the $4f \rightarrow 5d$ transitions

Peak	I_{the} (a. u)	I_{exp} (a. u)
1	1.4	1.4
2	0.36	0.38
4	0.46	0.78
6	1.28	1.36
7	1.3	1.3

I_{exp}, experimental intensity; I_{the}, theoretical intensity.

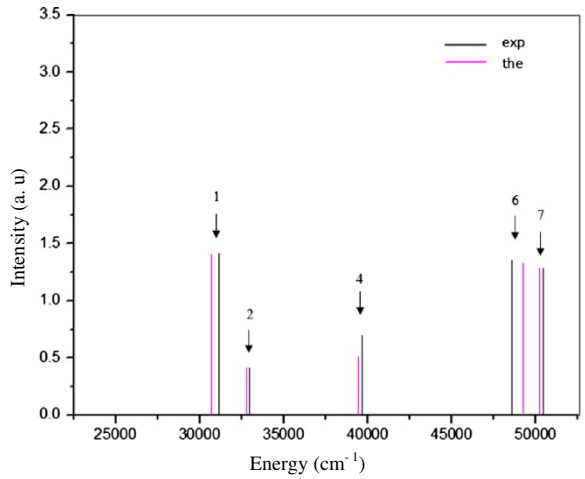

Figure 5 Experimental and theoretical absorption lines of the Ce^{3+}in YAB.

bands for which we have obtained a good agreement between experimental and theoretical results (Table 4, Figure 5).

Emission spectra

The room-temperature emission spectrum of YAB:Ce^{3+} excited at 274 nm is presented in the 300- to 440-nm spectral range (approximately 22,000 to 34,000 cm^{-1}) (Figure 6). This spectrum is badly resolved, and it shows the contribution of $^2F_{5/2}$ and $^2F_{7/2}$ multiplets, corresponding to transitions from the $5d^1$ fundamental state to the F_1, F_2, F_3, F_4, F_5, F_6, and F_7 Stark levels stemming from $4f^1$ configuration. It consists of a broad band with a double structure.

High-resolution polarized emission from the ^2D least excited to the $^2F_{5/2}$ ground state measured at 4 K indicates a splitting of this state into three levels. To determine the decomposition of Stark levels stemming from $^2F_{5/2}$ and $^2F_{7/2}$ multiplets, Watterich et al. [8] used a polarized emission spectrum of cerium in YAB realized at 4 K (Figure 7). Three various bands are detected: two σ bands for E ⊥ [0001] and a π band for E//[0001] [8]. This high-resolution polarized emission spectrum indicates that the $^2F_{5/2}$ state possesses three constituents. The second level is then located at 277 ± 18 cm^{-1} above the fundamental level, and the third is located at 140 ± 10 cm^{-1} above the second one.

On the basis of these data, Watterich et al. [8] have proposed a schematic energy level system for Ce^{3+} in D_3 symmetry site. However, these levels were not characterized with respect to symmetry type, and no attempt was made to analyze the observed energy level structure in terms of model crystal field Hamiltonian.

Based on our recent works on rare earth ions in YAB, Er^{3+} [9], Yb^{3+} [10], and Tm^{3+} [11], we have determined the crystal field parameters of Ce^{3+} ion in YAB by considering the general trend of these CF parameters with the ionic radius of the rare earth ions [11]. This general trend allows the prevision of the emission ranges of each rare earth ions in the YAB host by calculating the crystal field parameters and then the theoretical Stark energy level diagram.

The calculated CF parameters of Ce^{3+} in YAB for the $4f$ level are reported in Table 5. Using these parameters, we have established a theoretical Stark energy level diagram of the Ce^{3+} ion (Table 6). The calculated values are in good agreement with the experimental diagram of the $^2F_{5/2}$ ground state determined by Watterich [8]. By considering the $^2F_{7/2}$ excited state, we have estimated the positions of all

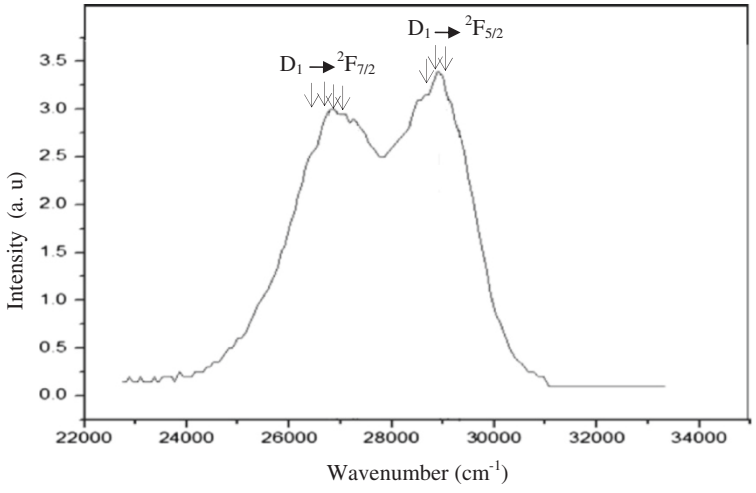

Figure 6 Emission spectrum of Ce^{3+}-doped YAB, measured at 300 K and excited at 274 nm [8].

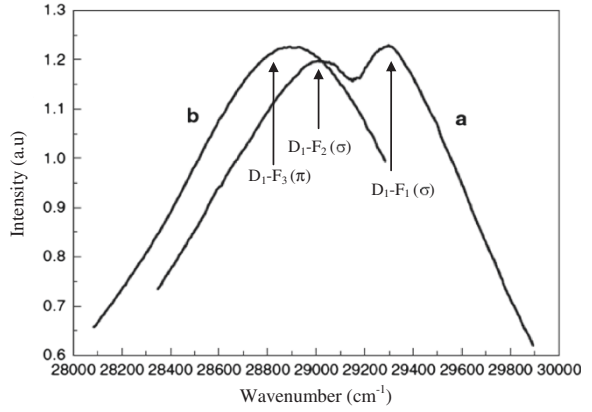

Figure 7 Polarized emission spectra of YAB:Ce^{3+}measured at high resolution (0.15 nm). (a) E ⊥ (0001) and **(b)** E//(0001) [8].

emissions from the ^2D ground state to the $^2F_{7/2}$ Stark levels. The calculated energies correspond well with the emission lines labeled in Figure 6.

The fitting procedure was then performed between the calculated and experimental Stark energy levels. The final set of the CFPs changed relatively little from the starting set (Table 6). Furthermore, the $D_1 \rightarrow {}^2F_{5/2}$ and $D_1 \rightarrow {}^2F_{7/2}$ transitions reported in Figure 6, which are not included in the fitting procedure, can be assigned using the calculated Stark energy levels of $^2F_{5/2}$ and $^2F_{7/2}$ reported in Table 6, confirming our assignment.

For the 5*d* excited level, the calculated crystal field parameters leading to the best fit between experimental and theoretical Stark energy levels are represented in Table 7. The comparison between theoretical and experimental energies is reported in Table 8.

Each level is calculated with its symmetry type $E_{1/2}$ or $E_{3/2}$ in D_3 double group. The consistency between the two sets of data is reasonable, and the calculated irreducible representations of the Stark levels reflect the polarization behavior of the corresponding transitions (Figure 8).

Table 5 Calculated crystal field and spin-orbit parameters (cm^{-1}) for the *f* electrons in YAB:Ce^{3+}

	$B_{kq}(f)$	
	Initial parameters (cm^{-1})	Calculated parameters (cm^{-1})
B_{20}	254	247
B_{40}	−1,081	−1,165
B_{43}	682	612
B_{60}	1,440	1,515
B_{63}	−877	−728
B_{66}	−560	−606
ξ_f	540	579

Table 6 Experimental and theoretical Stark energy levels (cm^{-1}) of 4*f* electron in YAB:Ce^{3+}crystal

^2F	E_{the} (cm^{-1})	E_{exp} (cm^{-1})	Irreducible representations
$^2F_{5/2}$	0	0	$E_{1/2}$
	241	241	$E_{1/2}$
	392	392	$E_{3/2}$
$^2F_{7/2}$	2,018	2,015	$E_{1/2}$
	2,253	2,258	$E_{3/2}$
	2,421	2,426	$E_{1/2}$
	2,588	2,587	$E_{1/2}$

E_{exp}, experimental Stark energy level; E_{the}, theoretical Stark energy level.

Verification of the polarized spectra

Knowing the symmetry site occupied by an ion in a given crystal, the group theory allows us to determine the number and symmetry of the Stark levels stemming from every multiplet $^{2S+1}L_J$. The resulting states are expressed by the full rotation compatibility of group table (Table 1). The selection rules for the electric dipole transition can then be deduced by group theory considerations and are listed in Table 2.

The calculated eigenstates of the 4*f* Stark energy levels are given by:

$$\begin{aligned} E_{\frac{1}{2}} : |\Psi_1\rangle = {} & \alpha_1\left|\frac{7}{2},\frac{7}{2}\right\rangle+\alpha_2\left|\frac{7}{2},\frac{5}{2}\right\rangle+\alpha_4\left|\frac{7}{2},\frac{1}{2}\right\rangle+\alpha_5\left|\frac{7}{2},-\frac{1}{2}\right\rangle \\ & +\alpha_7\left|\frac{7}{2},-\frac{5}{2}\right\rangle+\alpha_8\left|\frac{7}{2},-\frac{7}{2}\right\rangle+\beta_1\left|\frac{5}{2},\frac{5}{2}\right\rangle \\ & +\beta_3\left|\frac{5}{2},\frac{1}{2}\right\rangle+\beta_4\left|\frac{5}{2},-\frac{1}{2}\right\rangle+\beta_6\left|\frac{5}{2},-\frac{5}{2}\right\rangle \end{aligned} \quad (12)$$

$$E_{\frac{3}{2}} : |\Psi_1\rangle = \alpha_3\left|\frac{7}{2},\frac{3}{2}\right\rangle+\alpha_6\left|\frac{7}{2},-\frac{3}{2}\right\rangle+\beta_2\left|\frac{5}{2},\frac{3}{2}\right\rangle+\beta_5\left|\frac{5}{2},-\frac{3}{2}\right\rangle \quad (13)$$

where the $|\Psi_1\rangle$ states are written in $|J, M_J\rangle$ representation, $M_J = J, J\text{-}1,\ldots,\text{-}J$ being the z projection of $J = 7/2, 5/2$, and α_i and β_j are reels.

Table 7 Calculated crystal field and spin-orbit parameters (cm^{-1}) for 5*d* electron in YAB:Ce^{3+} crystal

	$B_{kq}(d)$	
	Initial parameters (cm^{-1})	Final parameters (cm^{-1})
B_{20}	10,519 [21]	25,754
B_{40}	−24,549 [21]	−28,764
B_{43}	-	457
F_0	30,000	40,542
ξ_d	1,140 [22]	1,083

Table 8 Experimental and theoretical energy levels (cm^{-1}) of 5*d* electrons in YAB:Ce^{3+}

	E_{the} (cm^{-1})	E_{exp} (cm^{-1})	Irreducible representations
$^2D_{3/2}$	30,670	31,152	$E_{3/2}$
	32,895	32,934	$E_{1/2}$
$^2D_{5/2}$	39,499	39,657	$E_{1/2}$
	49,341	48,561	$E_{3/2}$
	50,302	50,535	$E_{1/2}$

The calculated eigensates of the 5*d* Stark energy levels are given by:

$$E_{\frac{1}{2}} : |\Psi_2\rangle = \alpha_1' \left|\frac{5}{2}, \frac{5}{2}\right\rangle + \alpha_3' \left|\frac{5}{2}, \frac{1}{2}\right\rangle + \alpha_4' \left|\frac{5}{2}, -\frac{1}{2}\right\rangle + \alpha_6' \left|\frac{5}{2}, -\frac{5}{2}\right\rangle + \beta_2' \left|\frac{3}{2}, \frac{1}{2}\right\rangle + \beta_3' \left|\frac{3}{2}, -\frac{1}{2}\right\rangle \quad (14)$$

$$E_{\frac{3}{2}} : |\Psi_2\rangle = \alpha_2' \left|\frac{5}{2}, \frac{3}{2}\right\rangle + \alpha_5' \left|\frac{5}{2}, -\frac{3}{2}\right\rangle + \beta_1' \left|\frac{3}{2}, \frac{3}{2}\right\rangle + \beta_4' \left|\frac{3}{2}, -\frac{3}{2}\right\rangle \quad (15)$$

where the $|\Psi_2\rangle$ states are written in $|J, M_J\rangle$ representation, $M_J = J, J\text{-}1, \ldots, -J$ being the z projection of $J = 5/2, 3/2$, and α_i' and β_j' are reels.

Using the symmetry type ($E_{1/2}$, $E_{3/2}$) of these wave functions, all the polarized spectra are confirmed (Figure 7). Indeed, the study of each wave function associated to 4*f* and 5*d* levels permits the determination of the allowed transitions between $^2F_{5/2}$ level (F_1, F_2, and F_3) Stark states and the $^2D_{3/2}$ (D_1) first excited state. We note the presence of two σ transitions ($^2D_{3/2} \rightarrow F_1$ and $^2D_{3/2} \rightarrow F_2$) and one π transition ($^2D_{3/2} \rightarrow F_3$). A schematic representation for these transitions is given in Figure 7.

Decay time of the $5d \rightarrow {}^2F_{5/2}$ transition

To calculate the decay time of Ce^{3+} luminescence in YAB crystal, it is necessary to calculate the oscillator strength, the effective section, and the $5d \rightarrow {}^2F_{5/2}$ probability transitions. For the $D_i \rightarrow {}^2F_{5/2}$ ($i = 1, 2, \ldots, 5$) transitions, the theoretical decay time, using equations presented in the section 'Theory', ends to the values reported in Table 9. The calculated values are in the same range compared with the experimental decay time (25 ns) measured for the Ce^{3+} in YAB for the $5d^1 \rightarrow {}^2F_{5/2}$ transition (340 nm) [20].

Conclusions

The optical spectra of Ce^{3+} ion doped in YAB crystal are investigated by presenting the various Hamiltonians which describe $4f \rightarrow 5d$ transitions. The 4*f* and 5*d* configuration energy levels and wave functions of Ce^{3+} in YAB crystal have been calculated using a model which includes spin-orbit coupling and crystal field interaction. The Stark energy levels have been obtained with their corresponding irreducible representations of D_3' double group. Calculated irreducible representations are in good agreement with theoretical prediction. Using the calculated eigenvector, the absorption peak

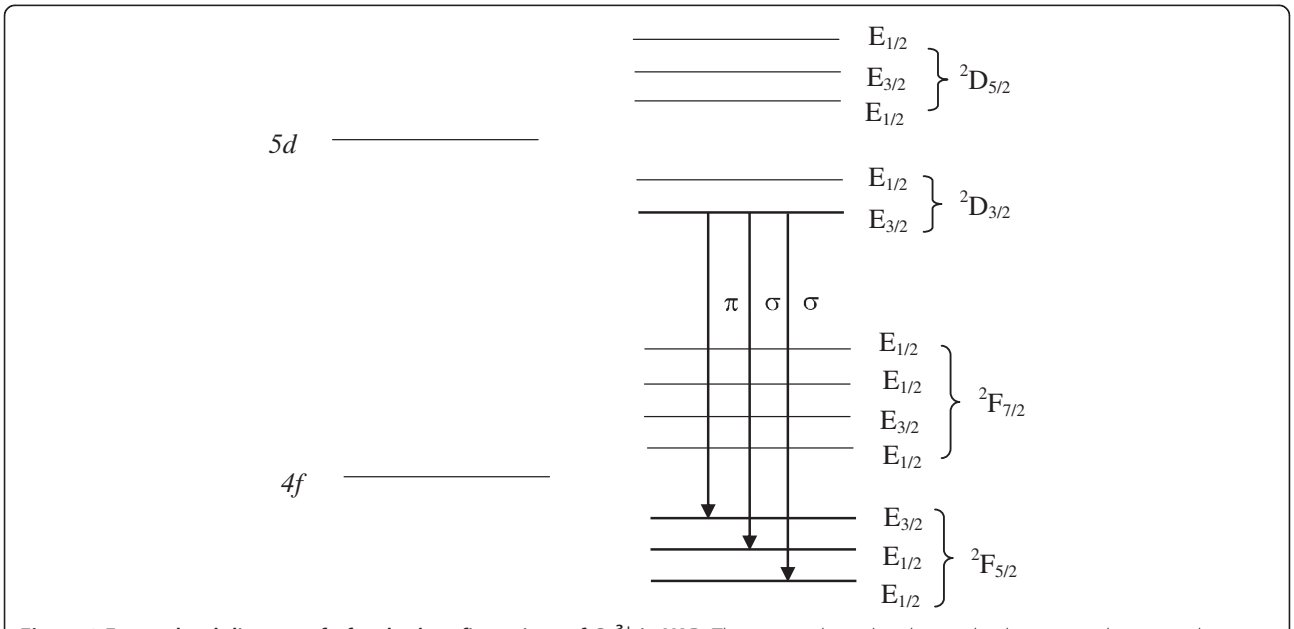

Figure 8 Energy level diagram of 4*f* and 5*d* configurations of Ce^{3+} in YAB. The arrows show the electric dipole permitted emission between $^2D_{3/2}$ and $^2F_{5/2}$ terms

Table 9 Calculated parameters for $5d \rightarrow {}^2F_{5/2}$ transition of Ce^{3+} in YAB host ($i = 1, 2, \ldots, 5$)

	F_{iF}	S_{iF} (m^2)	A_{iF}	τ_i (ns)
D_1	8.92110^{-5}	$5.363\ 10^{-22}$	1.92610^{8}	5.2
D_2	2.2210^{-5}	1.2410^{-22}	5.510^{7}	18.2
D_3	3.0310^{-5}	1.4110^{-22}	1.0810^{8}	9.2
D_4	7.8410^{-5}	2.9310^{-22}	4.3810^{8}	2.3
D_5	8.0310^{-5}	2.9410^{-22}	4.6610^{8}	2.14

intensities are reasonably well simulated. Previous assignment of the $5d$ electronic energies in YAB:Ce^{3+} is critically examined, and in light of the new energy level and transition intensity calculations, a revised assignment is put forward for the $5d$ energy levels. The calculated relative intensities of the profiles, as well as the decay time of the $5d \rightarrow {}^2F_{5/2}$ transitions, are in accordance with the experimental values.

Methods

We have carried out theoretical analyses of the optical spectra of Ce^{3+} ion doped in YAB crystal. A simulation program was developed in order to calculate the f and d electrons' crystal field energy levels in a crystalline host. This program written in C language was developed to calculate the theoretical Eigen states and the line intensities of the $f \rightarrow d$ transitions and then the decay time $5d \rightarrow {}^2F_{5/2}$ transitions.

Competing interests

The authors declare that they have no competing interests.

Authors' contributions

MD has developed the theoretical part and the simulation program. IK has performed the calculation and also analyzed the optical spectra and the results. Both authors have read the full manuscript and approved it for publication.

Authors' information

IK is an assistant at Sfax Preparatory Institute. MD holds the position as professor in the Department of Physics (Sfax Science Faculty Tunisia).

Received: 6 May 2012 Accepted: 6 September 2012
Published: 2 October 2012

References

1. Krupa, JC, Queffelec, M: UV and VUV optical excitations in wide band gap materials doped with rare earth ions: 4f–5d transitions. J. Alloys Comp. **250**, 287–292 (1997)
2. Ning, L, Duan, C, Xia, S, Reid, M, Tanner, P: A model analysis of $4f^N$–$4f^{N-1}5d$ transitions of rare-earth ions in crystals. J. Alloys Comp **366**, 34–40 (2004)
3. Dorenbos, P: The $4f^n \leftrightarrow 4f^{n-1}5d$ transitions of the trivalent lanthanides in halogenides and chalcogenides. J. Lumin. **91**, 91–106 (2000)
4. Dorenbos, P: The 5d level positions of the trivalent lanthanides in inorganic compounds. J. Lumin. **91**, 155–176 (2000)
5. Jacobs, R, Krupke, WF, Weber, MJ: Measurement of exited-state-absorption loss for Ce^{3+} in $Y_3A_{l1}O_{12}$ and implications for tunable 5d-4f rare earth lasers. Appl. Phys. Lett. **33**, 410–412 (1978)
6. Lin, HH, Liang, HB, Tian, ZF, Wang, J, Su, Q, Zhang, GB: Luminescence of Ba2Ca(BO3)2: Ce3 + —influence of charge compensator, energy transfer and LED application. J. Phys D. **42**, 165409 (2009)
7. Liu, XM, Lin, J: Synthesis and characterization of monodisperse spherical core-shell structured $SiO_2@Y_3Al_5O_{12}:Ce^{3+}/Tb^{3+}$ phosphors for field emission displays. J. Nanopart Res. **9**, 869–875 (2007)
8. Watterich, A, Aleshkevych, P, Borowiec, MT, Zayarnyuk, T, Szymczak, H, Beregi, E, Kovacs, L: Optical and magnetic spectroscopy of rare-earth-doped yttrium aluminium borate ($YAl_3(BO_3)_4$) single crystals. J. Phys. Condens. Matter **15**, 3323–3331 (2003)
9. Dammak, M: Crystal-field analysis of Er^{3+} ions in yttrium aluminium borate (YAB) single crystals. J Alloys Comp **393**, 51–56 (2005)
10. Dammak, M., Maalej, R, Kamoun, S, Kamoun, M: Investigations of the optical spectra and EPR parameters for Yb^{3+} ion in ($YAl_3(BO_3)_4$) crystals. J. Alloys Comp. **426**, 43–45 (2006)
11. Kebaili, I, Dammak, M, Cavalli, E, Bettinelli, M: Energy levels and crystal-field analysis of Tm^{3+} in $YAl_3(BO_3)_4$crystals. J. Luminescence **131**, 2010–2015 (2011)
12. Belokoneva, EL, Azizov, AV, Leonyuk, NI, Simonov, MA, Belov, NV: Crystal structure of $YaI_3[BO_3]_4$. Zh Strukt Khim **22**, 196–199 (1981)
13. Li, J, Wang, J, Cheng, X, Hu, X, Wang, X, Zhao, S: Growth, optical properties and defects of Tb:YAl3(BO3)4 crystal. Mater. Lett. **58**, 1096–1099 (2004)
14. Cavalli, E, Bovero, E, Magnani, N, Ramirez, MO, Speghini, A, Bettinelli, M: Optical spectroscopy and crystal-field analysis of YAl sub 3 (BO sub 3) sub 4 single crystals doped with dysprosium. J. Phys. Condens. Matter **15**, 1047–1056 (2003)
15. Ning, L, Jiang, Y, Xia, S, Tanner, P: Theoretical analysis and intensity calculation for the f → d absorption spectrum of U^{3+} in the LiY F_4 crystal. J Physics: Condensed Matter **15**, 7337–7350 (2003)
16. Ginzburg, VL: Theoretical physics and astrophysics. Pergamon, Oxford (1979)
17. Aminov, LK, Kaminskii, AA, Malkin, BZ: Physics and spectroscopy of laser crystals, p. 84. Nauka, Moscow (1986)
18. Sobel'man, II: Introduction to the theory of atomic spectra, p. 25. Nauka, Moscow (1977)
19. Malakhovskii, AV, Edelman, IS, Sokolov, AE, Temerov, VL, Bezmaternykh, LN, Sukhachov, AL, Seredkim, VA, Gnatchenko, SL, Kachur, IS, Piryatinskaya, VG: Polarized absorption spectra and spectroscopic parameters of Tm^{3+} in the $TmAl_3(BO_3)_4$ single crystal. Phy. Solid State **50**, 1278–1291 (2008)
20. Aloui-Lebbou, O, Goutauder, C, Kubota, S, Dujardin, C, Cohen-Adad, MT, Pédrini, C, Florian, P, Massiot, D: Structural and scintillation properties of new Ce^{3+}-doped alumino-borate. Opt. Mater. **16**, 77–86 (2001)
21. Reid, MF, Pieterson, L, Wegh, RT, Meijerink, A: Spectroscopy and calculations for4 $f^N \rightarrow 4\ f^{N-1}$ 5d transitions of lanthanide ions in LiYF4. Phys. Rev. B. **62**, 14744–14749 (2000)
22. Williams, GM, Becker, PC, Edelstein, N, Boatner, LA, Abraham, MM: Excitation profiles of resonance electronic Raman scattering in $ErPO_4$ crystals. Phys. Rev. B. **40**, 1288–1296 (1989)

doi:10.1186/2251-7235-6-21
Cite this article as: Kebaïli and Dammak: **Theoretical analysis and intensity calculation for the $f \rightarrow d$ absorption spectrum of Ce^{3+} in $YAl_3(BO_3)_4$ crystal.** *Journal of Theoretical and Applied Physics* 2012 **6**:21.